

Multinucleon transfer in the interaction of 977 MeV and 1143 MeV ^{204}Hg with ^{208}Pb V. V. Desai, A. Pica , W. Loveland , and J. S. Barrett*Department of Chemistry, Oregon State University, Corvallis, Oregon 97331, USA*

E. A. McCutchan

*National Nuclear Data Center, Brookhaven National Laboratory, Upton, New York 11973, USA*S. Zhu,^{*} A. D. Ayangeakaa,[†] M. P. Carpenter, J. P. Greene , and T. Lauritsen*Physics Division, Argonne National Laboratory, Argonne, Illinois 60439, USA*

R. V. F. Janssens

*Department of Physics and Astronomy, University of North Carolina at Chapel Hill, Chapel Hill, North Carolina 27599, USA
and Triangle Universities Nuclear Laboratory, Duke University, Durham, North Carolina 27708, USA*

B. M. S. Amro

Department of Physics, University of Massachusetts Lowell, Lowell, Massachusetts 01854, USA

W. B. Walters

Department of Chemistry, University of Maryland, College Park, Maryland 20742, USA

(Received 21 December 2019; accepted 9 March 2020; published 19 March 2020)

A previous study of symmetric collisions of massive nuclei has shown that current models of multinucleon transfer (MNT) reactions do not adequately describe the transfer product yields. To gain further insight into this problem, we have measured the yields of MNT products in the interaction of 977 ($E/A = 4.79$ MeV) and 1143 MeV ($E/A = 5.60$ MeV) ^{204}Hg with ^{208}Pb . We find that the yield of multinucleon transfer products are similar in these two reactions and are substantially lower than those observed in the reaction of 1257 MeV ($E/A = 6.16$ MeV) $^{204}\text{Hg} + ^{198}\text{Pt}$. We compare our measurements with the predictions of the GRAZING-F, dinuclear systems (DNS), and improved quantum molecular dynamics (ImQMD) models. For the observed isotopes of the elements Au, Hg, Tl, Pb, and Bi, the measured values of the MNT cross sections are orders of magnitude larger than the predicted values. Furthermore, the various models predict the formation of nuclides near the $N = 126$ shell, which are not observed.

DOI: [10.1103/PhysRevC.101.034612](https://doi.org/10.1103/PhysRevC.101.034612)**I. INTRODUCTION**

Multinucleon transfer (MNT) reactions are thought to be useful paths for synthesizing new n -rich heavy nuclei [1,2] and as possible paths for synthesizing nuclei near the $N = 126$ shell closure (of interest to the studies of r -process nucleosynthesis [3]). Some of the most interesting of these reactions involve the near-symmetric collisions of massive nuclei, such as $^{238}\text{U} + ^{248}\text{Cm}$. In this regard, the recent result of Welsh *et al.* [4] is somewhat disturbing. Welsh *et al.* measured the yields of several nuclides from the near-symmetric reaction of 1257 MeV ^{204}Hg with ^{198}Pt . They found that the yields of the transfer products were significantly larger, even for small transfers,

than those predicted by typical models for MNT reactions, such as GRAZING, the dinuclear systems (DNS) model, and the improved quantum molecular dynamics (ImQMD) model. While it is encouraging to see the larger than expected yields of the MNT products, it is vexing that we are unable to predict these yields even for the smallest transfers, let alone the larger ones. Accordingly, we undertook an investigation, reported in this paper, of the projectile-like fragments (PLFs) and target-like fragments (TLFs) yields in another symmetric reaction, the reaction of 977 and 1143 MeV ^{204}Hg with ^{208}Pb . By making this investigation, we hope to check whether there are some special features of near-symmetric collisions that affect the MNT yields.

II. EXPERIMENTAL

The experimental method used was similar to that of Desai *et al.* [5]. Using the Gammasphere facility of the Argonne National Laboratory, beams of ^{204}Hg struck targets of ^{208}Pb .

^{*}Present address: National Nuclear Data Center, Brookhaven National Laboratory, Upton, New York 11973, USA.

[†]Present address: United States Naval Academy, Annapolis, Maryland 21402 USA.

For the irradiation at 977 MeV, the effective target thickness was 19.5 mg/cm² and the total bombardment time was 1404 min. For the irradiation at 1143 MeV, the effective target thickness was 28.0 mg/cm² and the total bombardment time was 2632 min. (In the 977 MeV study, the actual beam energy was 1360 MeV. The incident beam loses energy as it goes through the target and after traversing 19.5 mg/cm² of ²⁰⁸Pb, the beam energy drops below the interaction barrier of 586.7 MeV. Thus, the “effective” target thickness was 19.5 mg/cm² while the physical target thickness was 48 mg/cm².) In the higher energy irradiation (1143 MeV), the incident beam energy was 1700 MeV, the physical target thickness was 44 mg/cm², and the effective target thickness was 27.7 mg/cm². The intensity of the beam was monitored periodically by inserting a suppressed Faraday cup in the beam line in front of the target. The beam intensities were 3.07×10^{10} and 3.17×10^{10} ions/min for the lower and higher energy irradiations, respectively. The lower energy irradiation was performed in May 2015, while the higher energy irradiation was performed in April 2016.

At the end of each irradiation, the target was removed from Gammasphere and γ -ray spectroscopy of the target radioactivities was carried out using a well-calibrated Ge detector in the Center for Accelerator Target Science (CATS) Counting Laboratory. The total observation period for the lower energy was 5 days, during which 25 measurements of target radioactivity were made. The total observation time for the higher energy was 7 days, during which 23 measurements of the sample were made. The analysis of these Ge γ -ray decay spectra was carried out using the FITZPEAKS [6] software. The end of bombardment (EOB) activities of the nuclides were used to calculate absolute production cross sections, taking into account the variable beam intensities using standard equations for the growth and decay of radionuclides during irradiation [7]. These measured absolute nuclidic production cross sections are tabulated in Tables I and II. These cross sections represent “cumulative” yields; i.e., they have not been corrected for the effects of precursor β decay. These cumulative yields are the primary measured quantity in this experiment.

To correct for precursor β decay, we have assumed that the β -decay-corrected independent yield cross sections for a given species, $\sigma(Z, A)$, can be represented as a histogram that lies along a Gaussian curve,

$$\sigma(Z, A) = \sigma(A) [2\pi C_Z^2(A)]^{-1/2} \exp\left[-\frac{(Z - Z_{mp})^2}{2C_Z^2(A)}\right], \quad (1)$$

where $\sigma(A)$ is the total isobaric yield (the mass yield), $C_Z(A)$ is the Gaussian width parameter for mass number A , and $Z_{mp}(A)$ is the most probable atomic number for that A . Given this assumption, the β -decay feeding correction factors for cumulative yield isobars can be calculated, once the centroid and width of the Gaussian function are known.

To uniquely specify $\sigma(A)$, $C_Z(A)$, and $Z_{mp}(A)$, one would need to measure three independent yield cross sections for each isobar. This is difficult and generally not feasible for most isobars. Instead, one assumes that the value of $\sigma(A)$ varies smoothly and slowly as a function of mass number

TABLE I. Fragment cumulative and independent yields for the reaction of ²⁰⁴Hg + ²⁰⁸Pb at $E_{lab} = 977$ MeV.

Isotope	σ_{CY} (mb)	σ_{IY} (mb)
⁷² Ga	0.078 ± 0.009	0.073 ± 0.009
⁸¹ Rb ^m	0.029 ± 0.020	0.024 ± 0.016
⁸⁵ Kr	0.052 ± 0.017	0.044 ± 0.014
⁹¹ Sr	0.080 ± 0.023	0.070 ± 0.020
⁹² Sr	0.183 ± 0.012	0.183 ± 0.018
⁹⁷ Zr	0.205 ± 0.010	0.205 ± 0.021
⁹⁰ Nb	0.159 ± 0.029	0.143 ± 0.026
⁹⁹ Mo	0.178 ± 0.001	0.178 ± 0.018
⁹³ Tc	0.21 ± 0.06	0.21 ± 0.06
⁹⁹ Tc	0.030 ± 0.009	0.023 ± 0.007
⁹⁷ Ru	0.751 ± 0.011	0.691 ± 0.069
¹⁰³ Ru	1.204 ± 0.082	0.773 ± 0.077
¹¹² Ag	0.232 ± 0.059	0.182 ± 0.046
¹¹⁵ Cd	0.130 ± 0.004	0.097 ± 0.010
¹¹⁷ Sb	0.585 ± 0.027	0.505 ± 0.051
¹³¹ I	0.082 ± 0.048	0.073 ± 0.043
¹²⁵ Xe	0.187 ± 0.011	0.161 ± 0.016
¹³⁵ Xe	0.079 ± 0.009	0.074 ± 0.008
¹⁴⁰ Ba	0.195 ± 0.020	0.180 ± 0.018
¹⁴³ Ce	0.099 ± 0.009	0.084 ± 0.008
¹⁵⁶ Sm	0.278 ± 0.035	0.278 ± 0.035
¹⁵⁴ Tb	0.737 ± 0.025	0.341 ± 0.034
¹⁶⁷ Ho	0.124 ± 0.019	0.106 ± 0.016
¹⁶⁹ Lu	0.221 ± 0.015	0.221 ± 0.022
¹⁸⁰ Hf ^m	0.095 ± 0.010	0.095 ± 0.010
¹⁸¹ Re	1.39 ± 1.05	1.39 ± 1.05
¹⁸² Re	1.883 ± 0.093	1.883 ± 0.188
¹⁸⁸ Re	0.219 ± 0.037	0.219 ± 0.037
¹⁹¹ Os	0.594 ± 0.031	0.281 ± 0.028
¹⁸⁸ Ir	0.192 ± 0.016	0.187 ± 0.019
¹⁹⁰ Ir	0.137 ± 0.005	0.068 ± 0.007
¹⁹⁵ Pt	0.918 ± 0.048	0.742 ± 0.074
¹⁹² Au	0.221 ± 0.007	0.190 ± 0.019
¹⁹³ Au	0.430 ± 0.072	0.357 ± 0.060
¹⁹⁴ Au	0.426 ± 0.043	0.426 ± 0.043
¹⁹⁶ Au	1.652 ± 0.028	0.804 ± 0.080
¹⁹⁸ Au	2.414 ± 0.010	1.930 ± 0.193
¹⁹⁹ Au	3.25 ± 0.02	2.65 ± 0.26
²⁰⁰ Au ^m	0.598 ± 0.026	0.598 ± 0.060
¹⁹⁵ Hg ^m	0.303 ± 0.011	0.273 ± 0.027
¹⁹⁷ Hg	0.897 ± 0.140	0.897 ± 0.140
²⁰³ Hg	38.1 ± 1.6	31.2 ± 3.1
¹⁹⁸ Tl	0.963 ± 0.080	0.847 ± 0.085
¹⁹⁹ Tl	0.870 ± 0.018	0.741 ± 0.074
²⁰⁰ Tl	2.21 ± 0.14	1.91 ± 0.19
²⁰¹ Tl	3.27 ± 0.03	2.59 ± 0.26
²⁰² Tl	3.14 ± 0.03	3.14 ± 0.31
²⁰⁰ Pb	0.388 ± 0.012	0.352 ± 0.035
²⁰¹ Pb	0.962 ± 0.077	0.845 ± 0.085

TABLE I. (Continued.)

Isotope	σ_{CY} (mb)	σ_{IY} (mb)
²⁰² Pb ^m	0.926 ± 0.015	0.926 ± 0.093
²⁰³ Pb	5.42 ± 0.02	4.45 ± 0.05
²⁰⁴ Pb	1.95 ± 0.18	1.418 ± 0.14
²⁰² Bi	0.412 ± 0.237	0.338 ± 0.020
²⁰³ Bi	0.577 ± 0.013	0.413 ± 0.041
²⁰⁴ Bi	0.786 ± 0.050	0.557 ± 0.056
²⁰⁵ Bi	1.87 ± 0.21	1.187 ± 0.133
²⁰⁶ Bi	1.53 ± 0.012	1.436 ± 0.144
²⁰⁶ Po	0.786 ± 0.078	0.594 ± 0.059
²⁰⁸ At	0.297 ± 0.128	0.234 ± 0.101
²⁰⁹ At	0.288 ± 0.005	0.205 ± 0.021
²¹⁰ At	0.396 ± 0.017	0.259 ± 0.026
²¹¹ Rn	0.560 ± 0.090	0.432 ± 0.069

and is roughly constant within any A range when determining $C_Z(A)$ and $Z_{mp}(A)$. The measured nuclidic formation cross sections are then placed in groups according to mass number. We assume that the charge distributions of neighboring isobaric chains are similar and radionuclide yields from a limited mass region can be used to determine a single charge distribution curve for that mass region. One can then use the laws of radioactive decay to iteratively correct the measured cumulative formation cross sections for precursor decay. These “independent yield” cross sections are also tabulated in Tables I and II. The cumulative and independent yield cross sections are similar because, without an external separation

TABLE II. Fragment cumulative and independent yields for the reaction of ²⁰⁴Hg + ²⁰⁸Pb at $E_{lab} = 1143$ MeV.

Isotope	σ_{CY} (mb)	σ_{IY} (mb)
⁶⁹ Zn	0.264 ± 0.017	0.264 ± 0.026
⁷² Zn	0.177 ± 0.033	0.176 ± 0.033
⁸² Br	0.329 ± 0.115	0.328 ± 0.115
⁸⁶ Y	0.083 ± 0.012	0.074 ± 0.010
⁸⁷ Y	0.373 ± 0.017	0.206 ± 0.020
⁹¹ Sr	0.886 ± 0.004	0.772 ± 0.077
⁹⁶ Nb	0.325 ± 0.010	0.325 ± 0.033
⁹⁵ Tc	0.047 ± 0.013	0.046 ± 0.013
⁹⁶ Tc	0.127 ± 0.014	0.127 ± 0.014
⁹⁷ Zr	1.246 ± 0.016	1.245 ± 0.125
⁹⁷ Ru	0.614 ± 0.008	0.565 ± 0.057
⁹⁹ Mo	1.974 ± 0.016	1.974 ± 0.197
¹⁰¹ Rh	0.050 ± 0.006	0.025 ± 0.003
¹⁰³ Ru	3.216 ± 0.006	0.639 ± 0.064
¹⁰⁵ Ru	0.773 ± 0.004	0.659 ± 0.141
¹¹¹ In	0.053 ± 0.003	0.049 ± 0.005
¹¹⁵ Cd	0.130 ± 0.040	0.085 ± 0.009
¹¹⁷ Sb	0.492 ± 0.029	0.532 ± 0.053
¹²⁰ Sb ^m	0.101 ± 0.015	0.100 ± 0.015
¹²² Sb	0.201 ± 0.020	0.200 ± 0.020
¹²⁸ Sb	0.321 ± 0.007	0.088 ± 0.043

TABLE II. (Continued.)

Isotope	σ_{CY} (mb)	σ_{IY} (mb)
¹³² Cs	0.214 ± 0.009	0.214 ± 0.021
¹³⁵ Ba ^m	0.759 ± 0.025	0.759 ± 0.076
¹⁴⁰ Ba	0.195 ± 0.020	0.172 ± 0.018
¹⁴³ Ce	0.210 ± 0.008	0.177 ± 0.018
¹⁴⁷ Gd	0.118 ± 0.047	0.114 ± 0.045
¹⁷² Er	0.159 ± 0.042	0.159 ± 0.042
¹⁶⁵ Tm	0.165 ± 0.010	0.138 ± 0.014
¹⁶⁹ Lu	0.377 ± 0.016	0.377 ± 0.038
¹⁷¹ Lu	0.946 ± 0.178	0.752 ± 0.142
¹⁷⁰ Hf	0.102 ± 0.041	0.096 ± 0.039
¹⁷³ Hf	0.436 ± 0.045	0.365 ± 0.039
¹⁸⁰ Hf ^m	0.088 ± 0.014	0.088 ± 0.014
¹⁷⁶ Ta	0.533 ± 0.094	0.433 ± 0.076
¹⁷⁷ Ta	0.824 ± 0.039	0.619 ± 0.062
¹⁷⁸ Ta	0.179 ± 0.050	0.179 ± 0.050
¹⁸³ Ta	0.221 ± 0.118	0.192 ± 0.102
¹⁸¹ Re	0.555 ± 0.051	0.454 ± 0.049
¹⁸² Re	0.686 ± 0.167	0.253 ± 0.147
¹⁸⁸ Re	0.716 ± 0.045	0.705 ± 0.071
¹⁸⁹ Re	1.19 ± 0.11	1.06 ± 0.11
¹⁸³ Os	0.196 ± 0.036	0.203 ± 0.021
¹⁸⁵ Os	1.370 ± 0.096	1.031 ± 0.103
¹⁸⁶ Ir	0.655 ± 0.147	0.552 ± 0.124
¹⁸⁸ Ir	0.587 ± 0.083	0.571 ± 0.081
¹⁹⁰ Ir	0.170 ± 0.052	0.161 ± 0.016
¹⁸⁸ Pt	0.748 ± 0.100	0.651 ± 0.087
¹⁹¹ Pt	1.76 ± 0.60	1.22 ± 0.41
¹⁹⁷ Pt ^m	0.89 ± 0.17	0.89 ± 0.17
¹⁹³ Au	0.43 ± 0.07	0.36 ± 0.06
¹⁹⁴ Au	0.430 ± 0.001	0.426 ± 0.043
¹⁹⁶ Au	1.652 ± 0.028	0.804 ± 0.080
¹⁹⁸ Au	2.414 ± 0.010	1.932 ± 0.193
¹⁹⁹ Au	3.25 ± 0.20	2.65 ± 0.26
²⁰⁰ Au ^m	0.598 ± 0.062	0.598 ± 0.060
¹⁹³ Hg ^m	0.574 ± 0.011	0.281 ± 0.028
¹⁹⁵ Hg ^m	1.08 ± 0.05	0.841 ± 0.085
¹⁹⁷ Hg	1.75 ± 0.13	1.75 ± 0.17
²⁰³ Hg	19.0 ± 0.5	17.5 ± 1.7
¹⁹⁷ Tl	1.53 ± 0.19	1.239 ± 0.152
¹⁹⁹ Tl	1.51 ± 0.24	1.05 ± 0.17
²⁰⁰ Tl	2.92 ± 0.15	2.09 ± 0.21
²⁰¹ Tl	4.70 ± 0.07	2.83 ± 0.28
²⁰² Tl	2.73 ± 0.03	2.72 ± 0.27
²⁰⁰ Pb	0.39 ± 0.01	0.31 ± 0.03
²⁰¹ Pb	0.962 ± 0.077	0.712 ± 0.071
²⁰² Pb ^m	0.926 ± 0.015	0.926 ± 0.092
²⁰³ Pb	1.92 ± 0.31	1.24 ± 0.20
²⁰³ Bi	1.19 ± 0.12	0.91 ± 0.09
²⁰⁴ Bi	1.27 ± 0.19	0.90 ± 0.13
²⁰⁵ Bi	2.79 ± 0.25	1.77 ± 0.18
²⁰⁶ Bi	1.81 ± 0.14	1.70 ± 0.17
²⁰⁶ Po	1.00 ± 0.15	0.75 ± 0.11
²⁰⁷ Po	1.00 ± 0.057	0.999 ± 0.100
²⁰⁹ At	1.12 ± 0.041	0.80 ± 0.08
²¹⁰ At	1.76 ± 0.27	1.15 ± 0.18
²¹¹ Rn	0.36 ± 0.09	0.28 ± 0.07

TABLE III. Summary of previous experiments on MNT reactions involving heavy nuclei.

Reaction	E_{lab} (MeV)	Reference
$^{18}\text{O} + ^{248}\text{Cm}$	95.5–96.5	[9]
$^{86}\text{Kr} + ^{248}\text{Cm}$	379–546	[9]
$^{136}\text{Xe} + ^{248}\text{Cm}$	624–868	[9]
$^{129}\text{Xe} + ^{248}\text{Cm}$	769–791	[10]
$^{132}\text{Xe} + ^{248}\text{Cm}$	793–817	[10]
$^{238}\text{U} + ^{197}\text{Au}$	1280–1561	[11]
$^{238}\text{U} + ^{238}\text{U}$	1280–1561	[11]
$^{64}\text{Ni} + ^{208}\text{Pb}$	350	[12]
$^{18}\text{O} + ^{208}\text{Pb}$	96	[13]
$^{136}\text{Xe} + ^{198}\text{Pt}$	1088	[14]
$^{136}\text{Xe} + ^{208}\text{Pb}$	743	[15]
$^{18}\text{O} + ^{238}\text{U}$	158	[16]
$^{136}\text{Xe} + ^{198}\text{Pt}$	761	[5]

of the reaction products by Z or A , one most likely detects only a single or a few nuclides for a given isobaric chain, and these nuclides are located near the maximum of the Gaussian yield distribution. The uncertainties in the calculated “independent yield” cross sections deduced in this manner have been examined by Morrissey *et al.* [8] and they have found a systematic uncertainty of $\pm 30\%$ associated with this procedure.

III. RESULTS AND DISCUSSION

Because of the nearly symmetric character of the $^{204}\text{Hg} + ^{208}\text{Pb}$ reaction, separation of the products into projectile-like fragments (PLFs) and target-like fragments

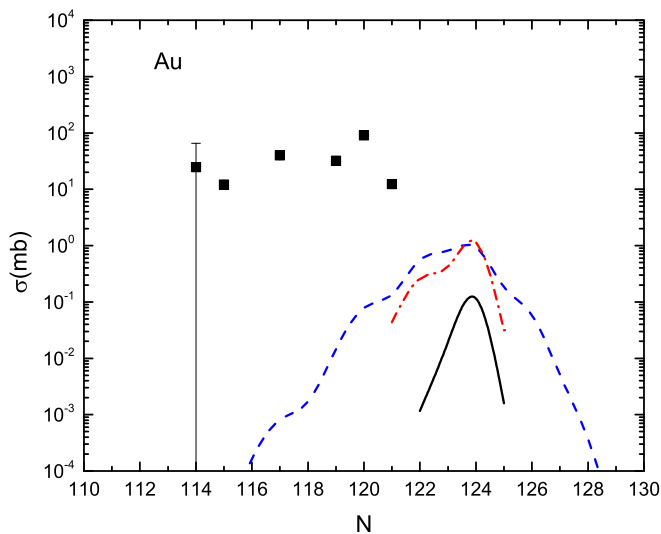


FIG. 1. A comparison of the predicted (GRAZING-F, DNS, and ImQMD) yields and the measured yields of the Au isotopes formed in the reaction of 977 MeV $^{204}\text{Hg}_{124}$ with $^{208}\text{Pb}_{126}$. The solid squares represent the experimental data, while the solid, dashed, and the dash-dotted lines represent the predictions of the GRAZING-F, DNS, and ImQMD models, respectively.

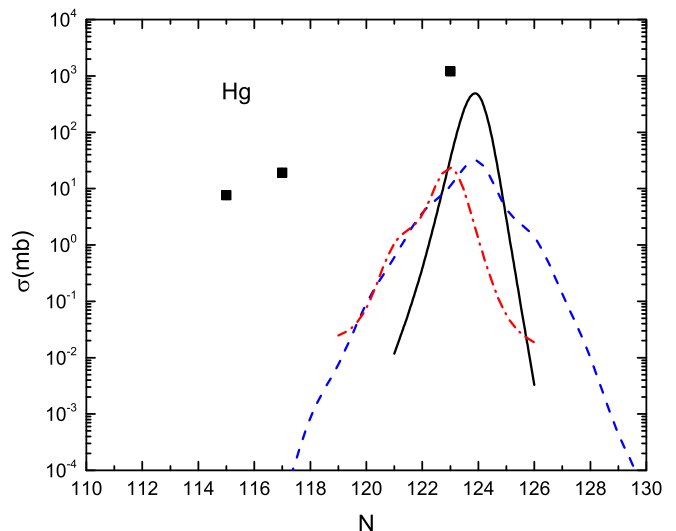


FIG. 2. A comparison of the predicted and measured yields of the Hg isotopes formed in the reaction of 977 MeV $^{204}\text{Hg}_{124}$ with $^{208}\text{Pb}_{126}$. See Fig. 1 for the meaning of the symbols.

(TLFs) is not meaningful. While some models for these reactions classify fragments as PLFs and TLFs, we have summed all of the predicted yields to give “fragment yields.”

A. Comparison with previous work

In Table III, we summarize previous studies of multinucleon transfer reactions involving heavy nuclei. The references are arranged chronologically. For further information, the reader is referred to these studies and review articles [17–19] describing previous work.

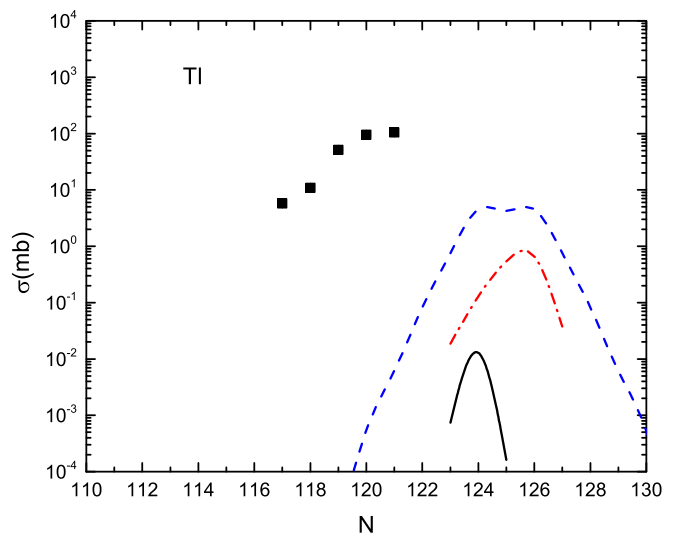


FIG. 3. A comparison of the predicted and measured yields of the Tl isotopes formed in the reaction of 977 MeV $^{204}\text{Hg}_{124}$ with $^{208}\text{Pb}_{126}$. See Fig. 1 for the meaning of the symbols.

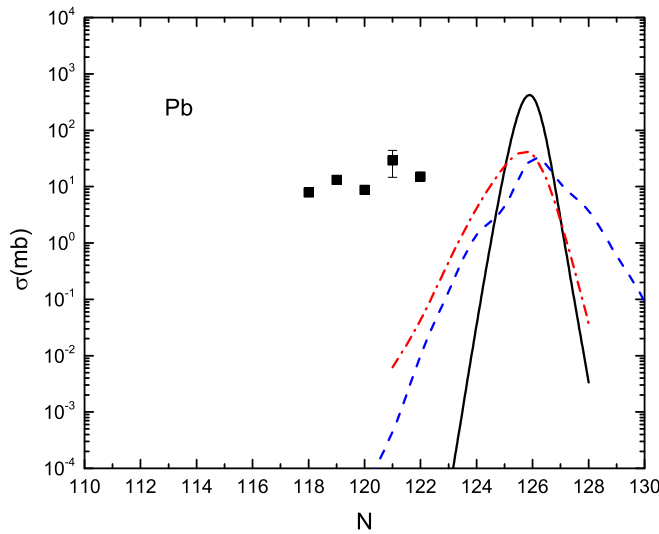


FIG. 4. A comparison of the predicted and measured yields of the Pb isotopes formed in the reaction of 977 MeV $^{204}\text{Hg}_{124}$ with $^{208}\text{Pb}_{126}$. See Fig. 1 for the meaning of the symbols.

B. Comparison with phenomenological models

A well-known model for predicting the cross sections for transfer products is GRAZING, a semiclassical model due to Pollarolo and Winther [20,21]. GRAZING uses a semiclassical model of the reacting ions moving on classical trajectories with quantum calculations of the probability of excitation of collective states and of nucleon transfer. This model describes few-nucleon transfers [22] well. It has been employed to describe the production of projectile-like fragments (PLFs) involving transfers of 45 nucleons in the asymmetric reaction of ^{136}Xe with ^{238}U , where the predictions of this model agree well with measurements [23]. Yanez and Loveland [24] have published a variant of the GRAZING code, called

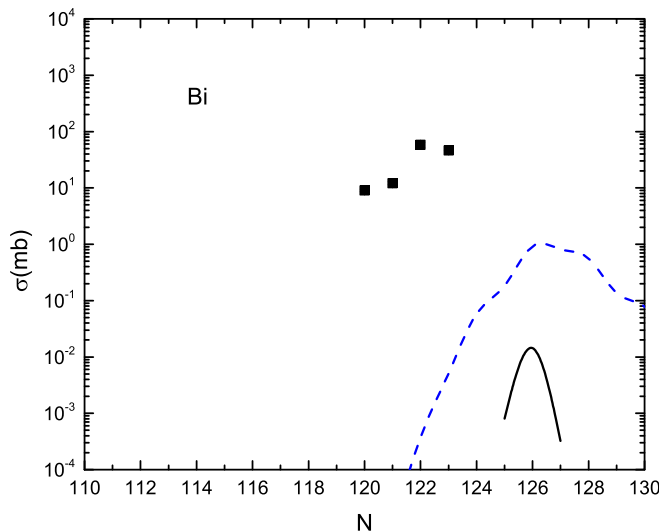


FIG. 5. A comparison of the predicted and measured yields of the Bi isotopes formed in the reaction of 977 MeV $^{204}\text{Hg}_{124}$ with $^{208}\text{Pb}_{126}$. See Fig. 1 for the meaning of the symbols.

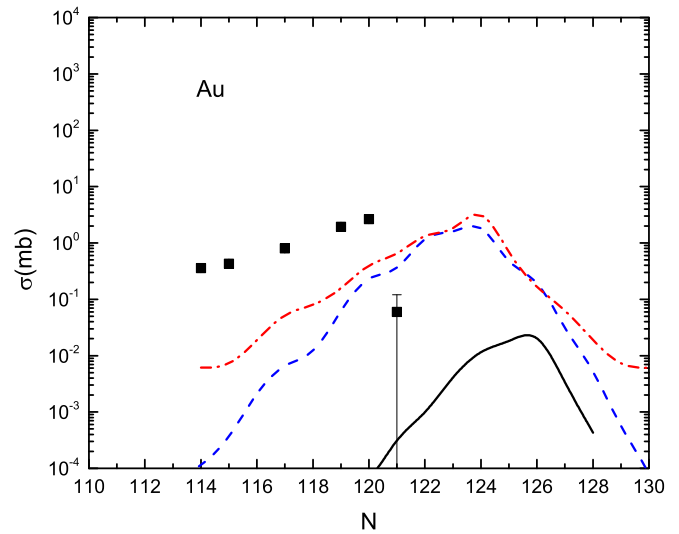


FIG. 6. A comparison of the predicted (GRAZING-F, DNS, and ImQMD) yields and the measured yields of the Au isotopes formed in the reaction of 1143 MeV $^{204}\text{Hg}_{124}$ with $^{208}\text{Pb}_{126}$. The solid squares represent the experimental data, while the solid, dashed and the dash-dotted lines represent the predictions of the GRAZING-F, DNS, and ImQMD models, respectively.

GRAZING-F, which takes into account the decay of the MNT primary fragments by both fission and neutron emission. The measured and predicted (GRAZING-F) values for selected nuclides are shown in Figs. 1–10.

Another model for predicting the yields of MNT products is the dinuclear system (DNS) model which is described in Refs. [25,26]. Unlike the GRAZING model, this model focuses on the more central collisions, in which there is considerable overlap between the colliding nuclei. The GRAZING and DNS models are, thus, complementary. The predictions

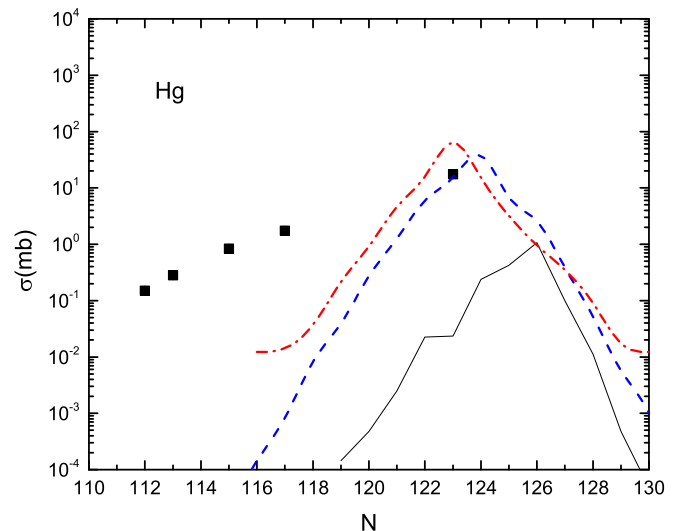


FIG. 7. A comparison of the predicted and measured yields of the Hg isotopes formed in the reaction of 1143 MeV $^{204}\text{Hg}_{124}$ with $^{208}\text{Pb}_{126}$. See Fig. 6 for the meaning of the symbols.

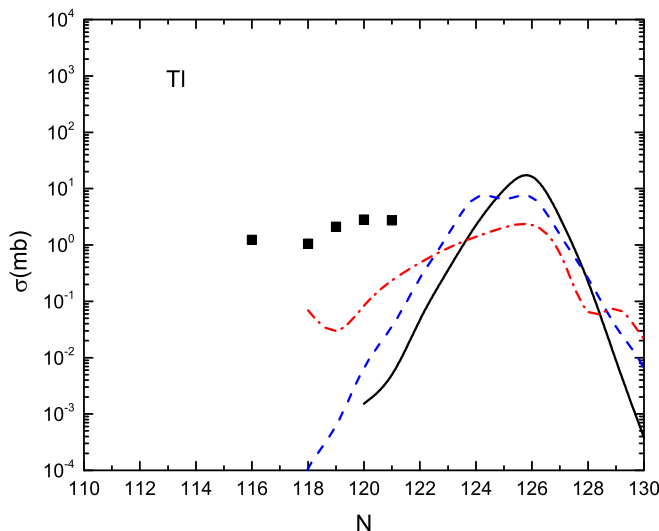


FIG. 8. A comparison of the predicted and measured yields of the Tl isotopes formed in the reaction of 1143 MeV $^{204}\text{Hg}_{124}$ with $^{208}\text{Pb}_{126}$. See Fig. 6 for the meaning of the symbols.

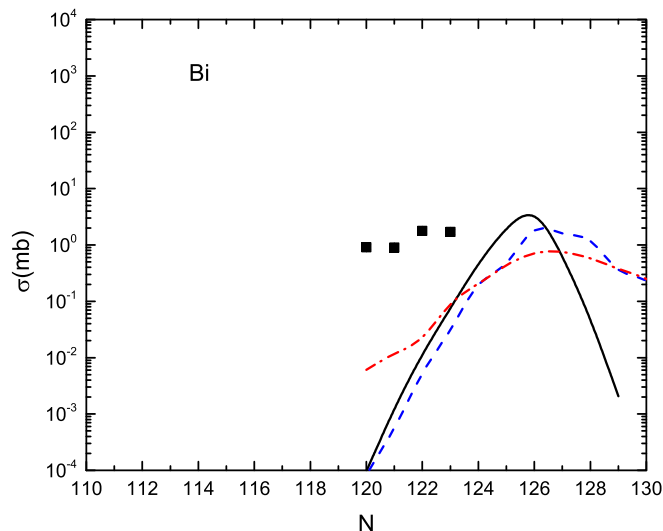


FIG. 10. A comparison of the predicted and measured yields of the Bi isotopes formed in the reaction of 1143 MeV $^{204}\text{Hg}_{124}$ with $^{208}\text{Pb}_{126}$. See Fig. 6 for the meaning of the symbols.

of the DNS model are compared to the measured data in Figs. 1–10, as well.

A third model for predicting MNT yields that has been quite successful [4,5] is the improved quantum molecular dynamics (ImQMD) model [27,28]. This model has been shown to describe MNT yields in a wide variety of reactions. The predictions of this model are also compared to the experimental data in Figs. 1–10.

One's first impression from Figs. 1–10 is that the increase in beam energy from 977 to 1143 MeV has a small effect on the measured cross sections.

In Figs. 1–10, the observed MNT products are more neutron deficient than those predicted by the models, with the exception of ^{203}Hg . The observed yields are orders of

magnitude larger than those predicted by the various models. As the atomic number of the elements increases, the various models predict large yields for the nuclei near the $N = 126$ shell—a prediction that is not consistent with the measurements. This nonobservation of n -rich ($N \approx 126$) products is consistent with the work of Welsh *et al.* [4], suggesting this is not an experimental artifact. (In our studies of the $^{136}\text{Xe} + ^{208}\text{Pb}$ reaction [15], we did observe $N = 126$ nuclei, albeit with cross sections about two orders below model predictions.) One can be encouraged or discouraged by this situation. The fact that the measured cross sections are larger than the predicted cross sections is encouraging for using

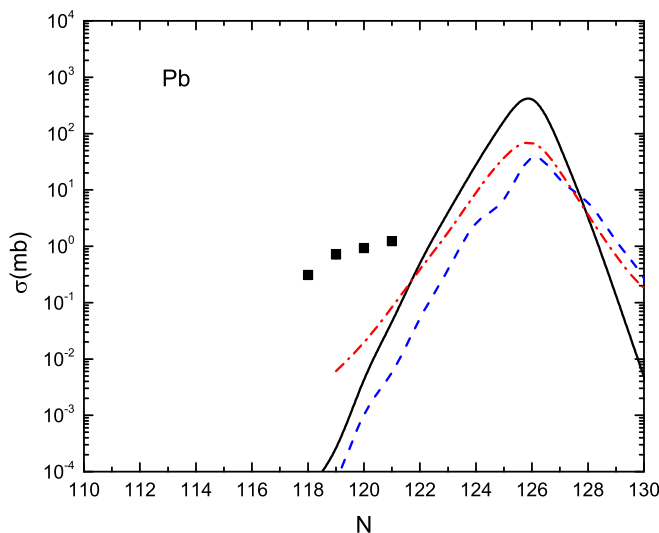


FIG. 9. A comparison of the predicted and measured yields of the Pb isotopes formed in the reaction of 1143 MeV $^{204}\text{Hg}_{124}$ with $^{208}\text{Pb}_{126}$. See Fig. 6 for the meaning of the symbols.

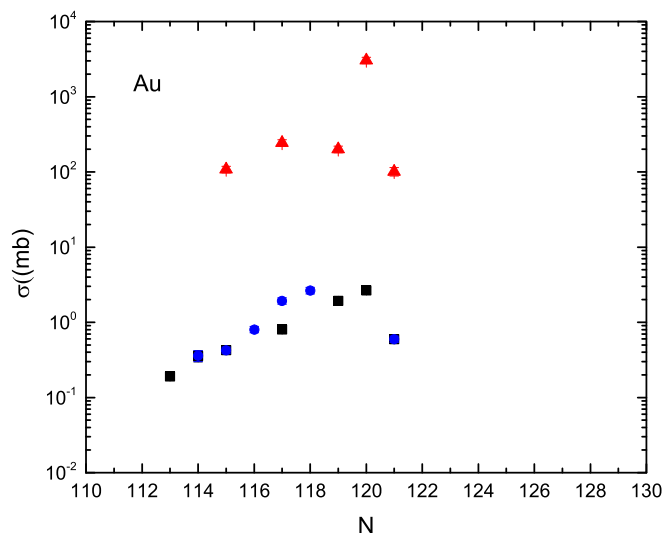


FIG. 11. A comparison of the yields of the Au transfer products in the reaction of 997 MeV $^{203}\text{Hg} + ^{208}\text{Pb}$ (this work, black squares), 1143 MeV $^{203}\text{Hg} + ^{208}\text{Pb}$ (this work, blue circles), and the reaction of 1257 MeV $^{203}\text{Hg} + ^{198}\text{Pt}$ [4] (red triangles).

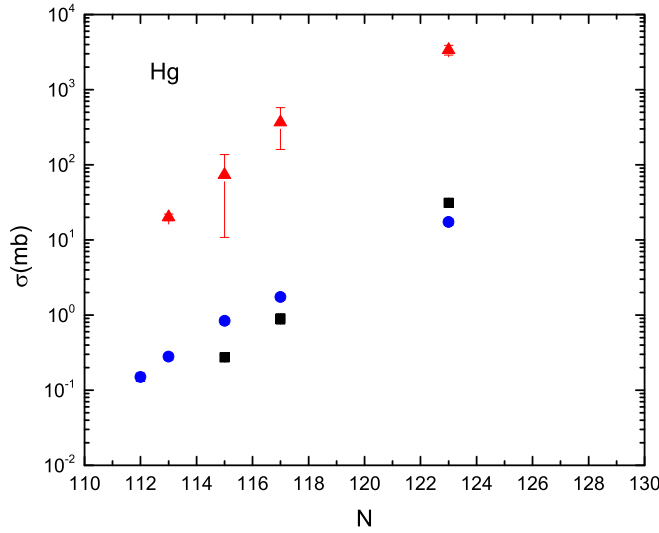


FIG. 12. A comparison of the yields of the Hg transfer products in the reaction of 997 MeV $^{203}\text{Hg} + ^{208}\text{Pb}$ (this work, black squares), 1143 MeV $^{203}\text{Hg} + ^{208}\text{Pb}$ (this work, blue circles), and the reaction of 1257 MeV $^{203}\text{Hg} + ^{198}\text{Pt}$ [4] (red triangles).

MNT reactions to synthesize new n -rich nuclei, but the inability to see nuclei near the $N = 126$ shell might indicate that these symmetric reactions are not a suitable path to these very n -rich nuclei. For all the models, there is an interesting “odd-even” effect with the atomic numbers of the MNT products. The even- Z nuclides (Hg and Pb) show higher yields than the odd- Z nuclides (Au, Tl, Bi) but one must remember Hg and Pb were the projectile and target, respectively.

If we compare the measured cross sections from this work (977 and 1143 MeV $^{204}\text{Hg} + ^{208}\text{Pb}$) with the measurements of Welsh *et al.* [4] for (1257 MeV $^{204}\text{Hg} + ^{198}\text{Pt}$) (Figs. 11–15), we observe similar yield patterns except that

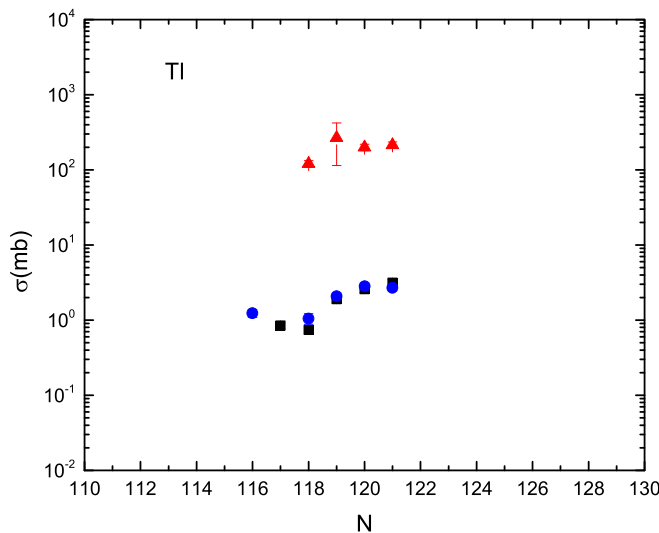


FIG. 13. A comparison of the yields of the Tl transfer products in the reaction of 997 MeV $^{203}\text{Hg} + ^{208}\text{Pb}$ (this work, black squares), 1143 MeV $^{203}\text{Hg} + ^{208}\text{Pb}$ (this work, blue circles), and the reaction of 1257 MeV $^{203}\text{Hg} + ^{198}\text{Pt}$ [4] (red triangles).

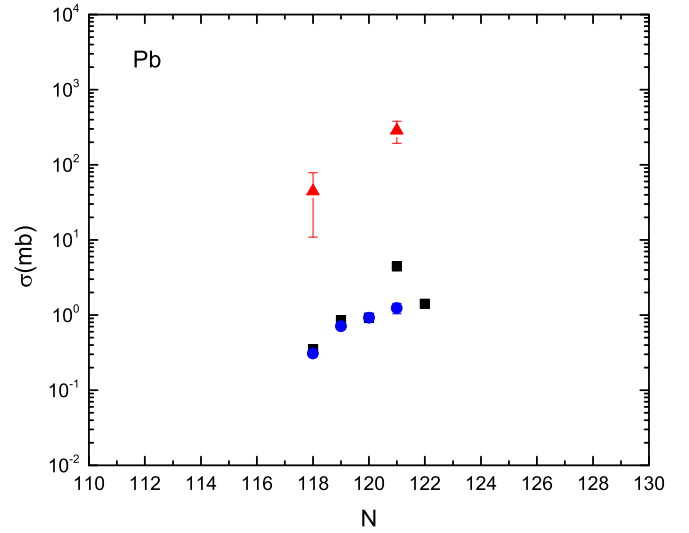


FIG. 14. A comparison of the yields of the Pb transfer products in the reaction of 997 MeV $^{203}\text{Hg} + ^{208}\text{Pb}$ (this work, black squares), 1143 MeV $^{203}\text{Hg} + ^{208}\text{Pb}$ (this work, blue circles), and the reaction of 1257 MeV $^{203}\text{Hg} + ^{198}\text{Pt}$ [4] (red triangles).

the cross sections for the higher energy reaction (1257 MeV $^{204}\text{Hg} + ^{198}\text{Pt}$) are substantially greater. It might be useful to make further measurements of the MNT yields with finer steps in the energy of the projectile and to distinguish between products emitted at the grazing angle and those emitted near 0° .

IV. CONCLUSIONS

What have we learned from this experiment? We found the following: (a) There is very little change in the yields of the MNT transfer products when the beam energy is raised

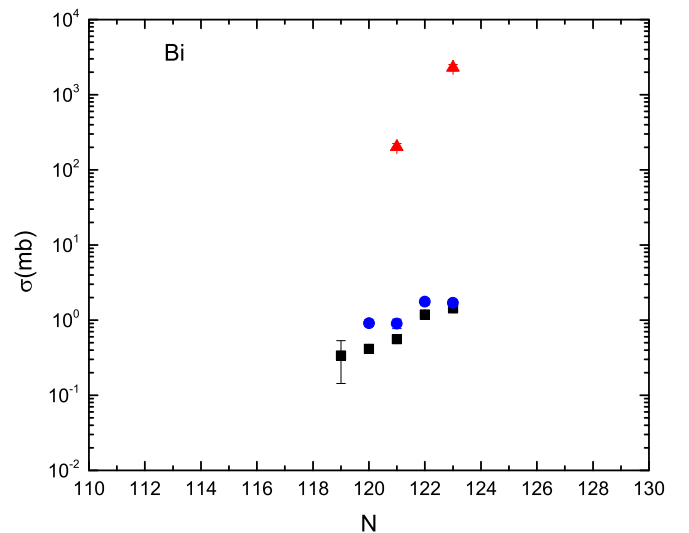


FIG. 15. A comparison of the yields of the Bi transfer products in the reaction of 997 MeV $^{203}\text{Hg} + ^{208}\text{Pb}$ (this work, black squares), 1143 MeV $^{203}\text{Hg} + ^{208}\text{Pb}$ (this work, blue circles), and the reaction of 1257 MeV $^{203}\text{Hg} + ^{198}\text{Pt}$ [4] (red triangles).

from 977 MeV to 1143 MeV ($E/A = 4.79$ to 5.60 MeV/A). (b) Comparing our results to those of Welsh *et al.* [4], we find that raising the projectile from 977 or 1143 MeV to 1267 MeV increases the MNT production cross sections by about two orders of magnitude. (c) The frequently used models for MNT collisions (GRAZING-F, DNS, and ImQMD) fail to describe these symmetric collisions, a situation similar to that observed by Welsh *et al.* [4]. This is not a trivial observation as symmetric reactions like U + Cm, etc., are frequently cited as pathways to n -rich heavy nuclei.

ACKNOWLEDGMENTS

This material is based upon work supported in part by the US Department of Energy, Office of Science, Office of Nuclear Physics under Awards No. DE-FG06-97ER41026 (OSU), No. DE-FG02-97ER41041 (UNC), No. DE-FG02-97ER41033 (TUNL), and No. DE-FG02-94ER40848 (UMassLowell) and Contracts No. DE-AC02-06CH11357 (ANL) and No. DE-AC02-98CH10886 (BNL). This research used resources of ANL's ATLAS facility, which is a DOE Office of Science User facility.

-
- [1] V. I. Zagrebaev and W. Greiner, *J. Phys. G* **34**, 1 (2007).
 [2] V. I. Zagrebaev and W. Greiner, *Phys. Rev. C* **83**, 044618 (2011).
 [3] V. I. Zagrebaev and W. Greiner, *Phys. Rev. Lett.* **101**, 122701 (2008).
 [4] T. Welsh, W. Loveland, R. Yanez, J. S. Barrett, E. A. McCutchan, A. A. Sonzogni, T. Johnson, S. Zhu, J. P. Greene, A. D. Ayangeakaa *et al.*, *Phys. Lett. B* **771**, 119 (2017).
 [5] V. V. Desai, W. Loveland, K. McCaleb, R. Yanez, G. Lane, S. S. Hota, M. W. Reed, H. Watanabe, S. Zhu, K. Auranen, A. D. Ayangeakaa *et al.*, *Phys. Rev. C* **99**, 044604 (2019).
 [6] <http://www.jimfitz.demon.co.uk/fitzpeak.htm>.
 [7] G. Friedlander, J. W. Kennedy, J. M. Miller, and E. Macias, *Nuclear and Radiochemistry*, 3rd ed. (Wiley, New York, 1981).
 [8] D. J. Morrissey, W. Loveland, M. de Saint Simon, and G. T. Seaborg, *Phys. Rev. C* **21**, 1783 (1980).
 [9] K. J. Moody, D. Lee, R. B. Welch, K. E. Gregorich, G. T. Seaborg, R. W. Loughheed, and E. K. Hulet, *Phys. Rev. C* **33**, 1315 (1986).
 [10] R. B. Welch, K. J. Moody, K. E. Gregorich, D. Lee, and G. T. Seaborg, *Phys. Rev. C* **35**, 204 (1987).
 [11] F. Funke, J. V. Kratz, N. Trautmann, N. Wiehl, G. Wirth, W. Bruchle, F. Wo, and K. Summerer, *Z. Phys. A* **340**, 303 (1991).
 [12] W. Krolas, R. Broda, B. Fornal, T. Pawlat, H. Grawe, K. H. Maier, M. Schramm, and R. Schubart, *Nucl. Phys. A* **724**, 289 (2003).
 [13] D. C. Biswas, P. Roy, Y. K. Gupta, B. N. Joshi, B. K. Nayak, L. S. Danu, B. V. John, R. P. Vind, N. Deshmukh, S. Mukherjee *et al.*, *J. Phys.: Conf. Ser.* **381**, 012091 (2012).
 [14] Y. X. Watanabe, Y. Hirayama, N. Imai, H. Ishiyama, S. C. Jeong, H. Miyatake, E. Clement, G. de France, A. Navin, M. Rejmund *et al.*, *Nucl. Instrum. Methods Phys. Res.* **317**, 752 (2013).
 [15] J. S. Barrett, W. Loveland, R. Yanez, S. Zhu, A. D. Ayangeakaa, M. P. Carpenter, J. P. Greene, R. V. F. Janssens, T. Lauritsen, E. A. McCutchan *et al.*, *Phys. Rev. C* **91**, 064615 (2015).
 [16] K. Nishio, K. Hirose, R. Léguillon, H. Makii, I. Nishinaka, R. Orlandi, J. Smallcombe, K. Tsukada, S. Chiba, T. Ohtsuki *et al.*, *Phys. Proced.* **64**, 140 (2015).
 [17] J. V. Kratz, W. Loveland, and K. J. Moody, *Nucl. Phys. A* **944**, 117 (2015).
 [18] F.-S. Zhang, C. Li, L. Zhu, and P. Wen, *Front. Phys.* **13**, 132113 (2018).
 [19] W. Loveland, *Front. Phys.* **7**, 23 (2019).
 [20] <http://personalpages.to.infn.it/~nanni/grazing/>.
 [21] A. Winther, *Nucl. Phys. A* **572**, 191 (1994); **594**, 203 (1995).
 [22] L. Corradi, G. Pollarolo, and S. Szilner, *J. Phys. G: Nucl. Part. Phys.* **36**, 113101 (2009).
 [23] A. Vogt *et al.*, *Phys. Rev. C* **92**, 024619 (2015).
 [24] R. Yanez and W. Loveland, *Phys. Rev. C* **91**, 044608 (2015).
 [25] L. Zhu, *Chin. Phys. C* **41**, 124102 (2017).
 [26] P.-w. Wen, C. Li, L. Zhu, C.-j. Liu, and F.-s. Zhang, *J. Phys. G: Nucl. Part. Phys.* **44**, 115101 (2017).
 [27] C. Li, F. Zhang, J. Li, L. Zhu, J. Tian, N. Wang, and F.-S. Zhang, *Phys. Rev. C* **93**, 014618 (2016).
 [28] C. Li, P. Wen, J. Li, G. Zhang, B. Li, X. Xu, Z. Liu, S. Zhu, and F.-S. Zhang, *Phys. Lett. B* **776**, 278 (2018).